A novel design of a hybrid glulam-steel substructure for the IEA 15-MW floating wind turbine

H H Yousef[1], Y Ma[1*], K S Patel[1] , and Y Xing[1]

[1] University of Stavanger, Norway

[*] yucong.ma@uis.no

Abstract. Wind energy has emerged as one of the most promising renewable energy sources. Furthermore, floating offshore wind turbines have enabled increased power generation in intermediate (45-150 m) and deep water (>150 m). However, the production, installation, and operation of wind turbines can produce considerable amounts of greenhouse gas emissions. This paper proposes a new hybrid glulam-steel floating substructure design for the IEA 15 MW floating wind turbine as an attempt to enhance the floating wind energy development with minimal cost and CO_2 footprint. The new design aims to replace steel with glued laminated timber (glulam) and presents a modified version of the UMaine VolturnUS-S semi-submersible platform that was initially developed for the IEA 15 MW turbine. First, Ansys workbench 2020 R1 is utilized to assess and then choose amongst three preliminary hybrid timber-steel models based on a set of criteria gathered from relevant timber and steel standards. In comparison to the UMaine VolturnUS-S semi-submersible platform, the selected hybrid design saves about 590 t of steel mass. Following that, a fully coupled aero-hydro-servo-elastic dynamic study is performed using OpenFAST to validate the chosen model. Only the ultimate limit state design (ULS) under normal and extreme operating conditions is considered. The results reveal that the glulam supporting structure is a good load-bearing solution for the IEA 15 MW turbine, with a utilization factor ranging from 74 to 94%.

1. Introduction

Engineers will be able to accomplish the net-zero emission target by 2050 if they develop more efficient wind turbines [1]. Most wind turbines installed offshore are bottom-fixed monopile wind turbines. As 80% of wind turbines are found in waters deeper than 60m, the bottom fixed wind turbine is not economical [2] whereas floating offshore wind turbine (FOWT) has an excellent advantage in deep waters. Floating wind turbines are designed to withstand extremely stochastic environmental loads for at least 20 years, according to International Electrotechnical Commission (IEC) specifications [3]. As the world shifts to renewable energy sources, more offshore wind farms are being built, necessitating the reduction of engineering, procurement, maintenance costs, and CO_2 footprint.

According to [4], the Carbon Intensity of Electricity (CIE), which ranges from 26.1 to 78.7 CO_2eq/kWh for a 6 MW raft-buoy wind turbine and a 6 MW spar buoy wind turbine, is found to be significantly dependent on the materials employed in both the manufacturing and maintenance procedures. The same study emphasizes the importance of creating new technologies to minimize the total steel mass to improve the turbine's environmental performance.

Glued laminated timber (glulam) is a strong, environmental-friendly, stable, and corrosion-resistant timber material that outperforms steel in many aspects including cost, strength-to-weight ratio, and

prefabrication possibility. Centuries of experience in building industries provide us with more knowledge regarding joint selection, limitations, and faster processes to construct with glulam [5]. In 2019, the Mjøstårnet 18-storey building was completed to be the highest in the world which is made completely of glulam [6]. In 2020, Modvion erected a 30-m-tall wooden tower in Björkö (Sweden) [7]. Recently, two firms (Stora Enso, a biomaterials and wood building firm, and Voodin Blade Technology GmbH, a German startup manufacturing wind turbine rotor blades) began partnering to produce wooden wind turbine blades to replace heavier non-renewable wind turbine blades.

The aim of this paper is to propose a new hybrid glulam-steel substructure for the IEA 15 MW wind turbine semi-submersible-type, see Figure 1. The selection of IEA 15 MW is based on the fact that it is a reference wind turbine that provides a solution that is viable today and, in the future [8]. First, 3 different hybrid models are modeled and analysed using ANSYS Workbench 2020 R1. The three configurations are compared to find the best solution that provides acceptable utilization factors at minimal material mass. Following that, a fully coupled aero-hydro-servo-elastic dynamic analysis is performed using OpenFAST to validate the chosen model. Only the ultimate limit state (ULS) design for the turbine under extreme and typical operating circumstances is examined.

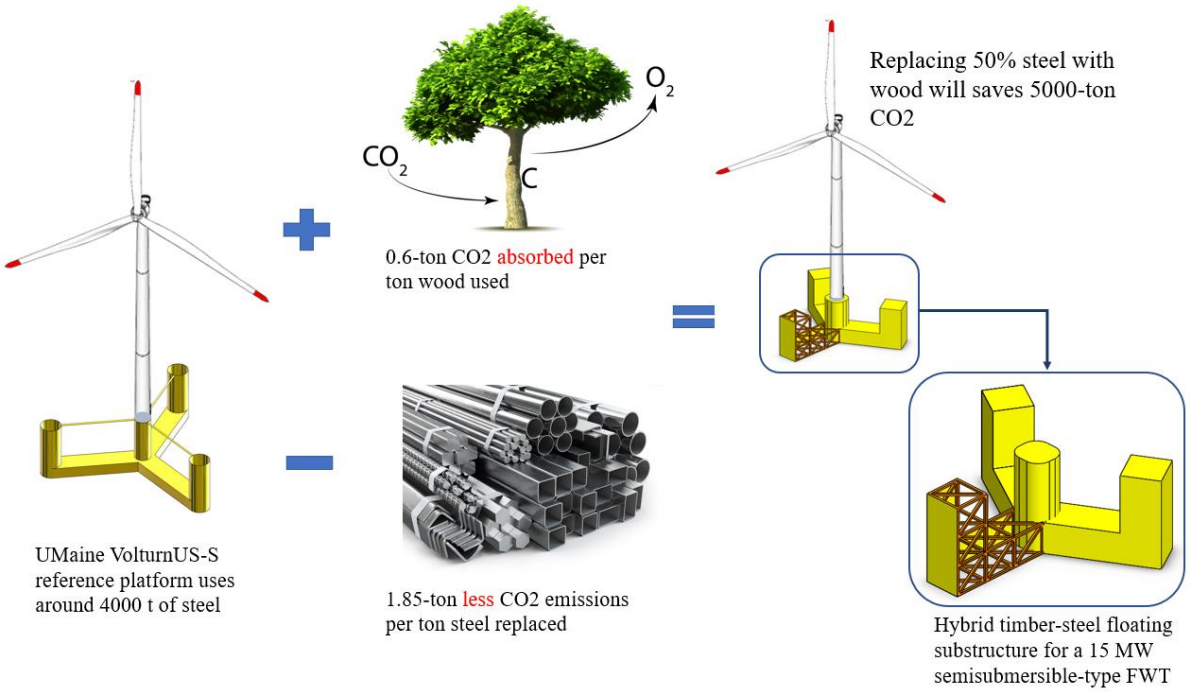

Figure 1. The environmental impact of using wood as a replacement for steel

2. System Description

The IEA 15-MW floating wind turbine (FWT) system [9] is used in this work. The FWT system will be expounded in two parts in the following sections. Firstly, the reference wind turbine will be described, then the properties of the original UMaine VolturnUS-S semi-submersible platform and the mooring system will be introduced.

2.1. IEA Wind 15-Megawatt reference FWT

In this paper, a 15-MW reference wind turbine (RWT) is used, the wind turbine was designed by International Electrotechnical Commission (IEC) Class 1B wind regime and is a conventional three-bladed, clockwise rotation-upwind turbine, equipped with a variable speed and collective pitch control system. The summary of the IEA Wind 15-MW RWT is shown in Table 1.

Table 1. General parameters of IEA Wind 15-MW RWT [8,9]

Parameter	**Value**	Units
Power rating	15	MW
Rotor orientation, configuration	Upwind, 3 blades	-
Control	Variable speed, collective pitch	-
Drivetrain	Low-speed, direct drive	
Cut-in, rated, cut-out wind speed	3, 10.59, 25	m/s
Rotor, hub diameter	240, 7.94	m
Hub height	150	m
Design tip-speed ratio	9	-
Minimum rotor speed	5	rpm
Maximum rotor speed	7.56	rpm
Maximum tip speed	95	m/s
Water depth	200	m
Total system mass	20,093	t
Platform mass	17,839	t
Rotor nacelle assembly mass	991	t
Tower mass	1,263	t
Tower base diameter	10	m

2.2. UMaine VolturnUS-S reference semi-submersible platform

This work utilizes the UMaine VolturnUS-S semi-submersible floating structure that is used to support the 15-MW RWT as a starting point to establish the new hybrid design. The floater comprises 3 columns that spread around a fourth central column. The columns are mounted on a star-shaped pontoon with a triangular cross-section at the bottom. The columns are also connected using three 0.9-m-diameter radial struts at the top. Three catenary mooring lines are used to maintain the floater in position, see Figure 2 (b). More details of the UMaine VolturnUS-S semi-floater and the mooring system are shown in Table 2 and Table 3, respectively.

Table 2. Semi-submersible Platform Properties [9]

Parameter	**Value**	**Units**
Hull displacement	20,206	m^3
Hull steel mass	3,914	t
Tower interface mass	100	t
Ballast mass (fixed/fluid)	2,540/11,300	t
Draft	20	m
Freeboard	15	m
Vertical center of gravity from SWL	-14.94	m
Vertical center of buoyancy from SWL	-13.63	m
Roll inertia about the center of gravity	1.251×10^{10}	$kg\cdot m^2$
Pitch inertia about the center of gravity	1.251×10^{10}	$kg\cdot m^2$
Yaw inertia about the center of gravity	2.367×10^{10}	$kg\cdot m^2$

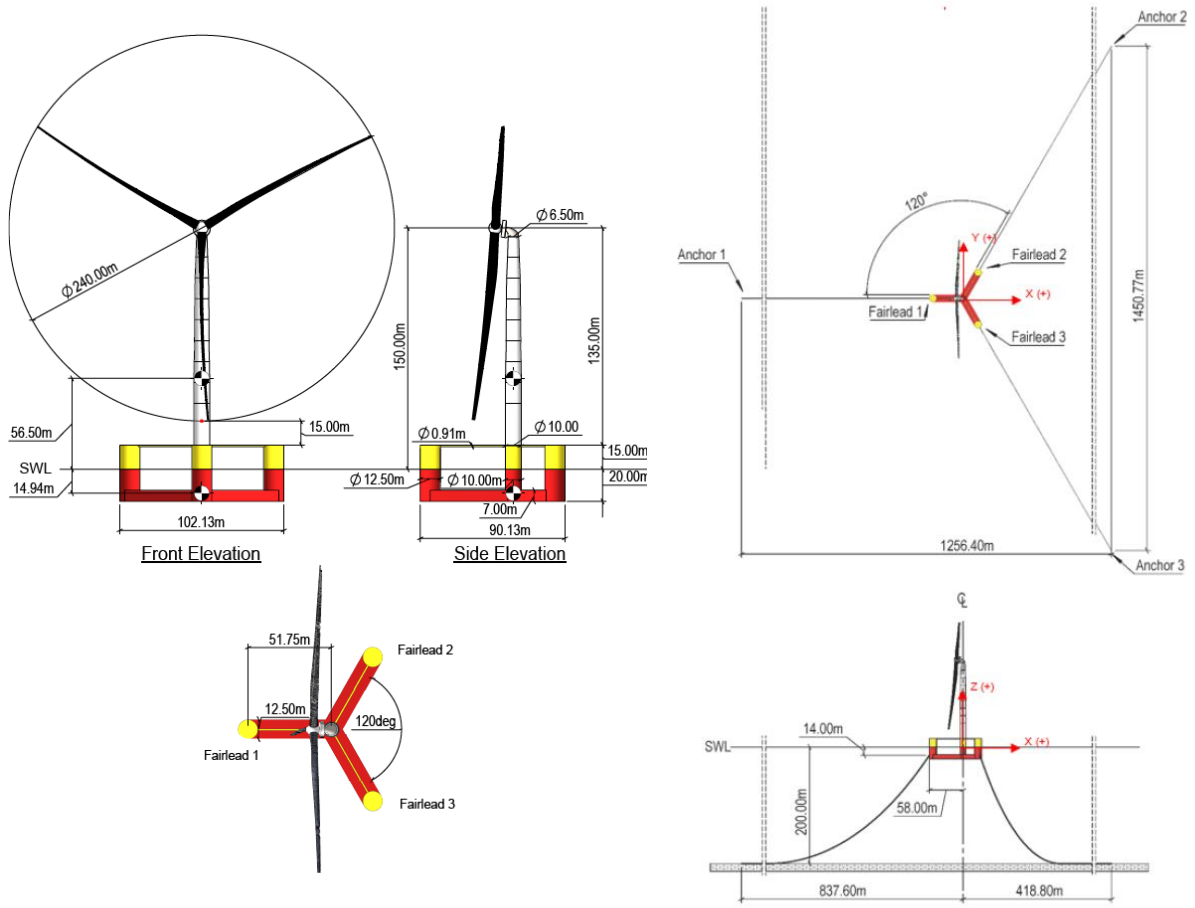

(a) (b)

Figure 2. (a) Main dimensions of the UMaine VolturnUS-S floater of the 15-MW wind turbine; (b) Sketch of the mooring system in the 15-MW FWT

Table 3. Mooring system's properties [9]

Parameter	Value	Units
System type & number of lines	Chain Catenary & 3 Lines	-
Line type	Studless R3 Chain	-
Line breaking strength	22.286	kN
Fairlead depth	14	m
Dry line linear density	685	kg/m
Extensional stiffness	3270	MN
Line unstretched length	850	m
Fairlead pretension	2,437	kN
Fairlead angle from SWL	56.4	deg

3. Finite Element Analysis of Three Concept Configurations

Three configurations are proposed for this work as shown in Figure 3. Since the floater is axisymmetric, the figure shows only the layout of the glulam supporting system for one pontoon and the central part where all 3 pontoons meet. Each of the configurations has similar external dimensions to the UMaine

platform, and the consists of 0.05 mm steel plates supported by different glulam supporting structures. More information regarding detailed dimensions is provided in Yousef (2023) Appendix A [10].

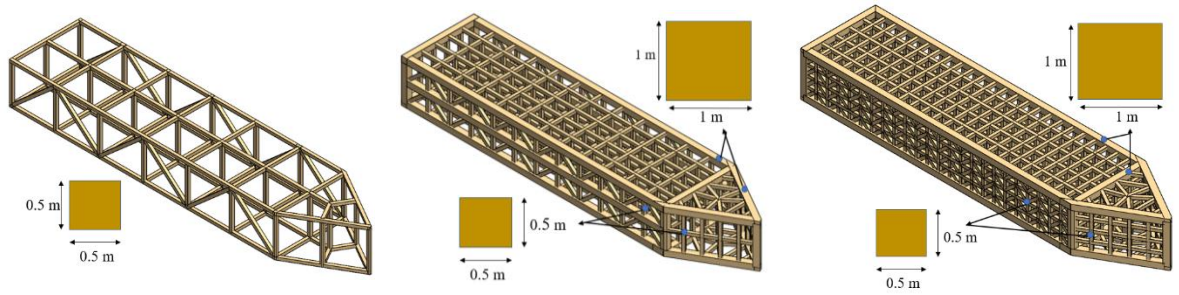

(a) (b) (c)

Figure 3. Glulam-based supporting structures for the three proposed configurations

3.1. Load and boundary conditions

To simplify the complexity of the design process, only the maximum aerodynamic load at rated wind velocity and hydrostatic pressure are considered. One pinned support was applied to one of the radial columns to simulate the behavior of the floater and allow for rotational motions only. Based on that, only the results obtained from the other two unsupported pontoons are valid. More information about loads and boundary conditions can be found in [10].

3.2. Material properties

Table 4 shows the material properties that were assigned for steel and glulam GL30h [11].

Table 4. Material properties of the plate's steel and glulam Gl30h assigned for the beams [11]

Property	**Glulam G30h for beams**	**Steel for plates**	**Unit**
Density	480	7850	kg/m^3
Young's Modulus X(L) direction	1.36×10^{10}		Pa
Young's Modulus Y(R) direction	3×10^{8}	2×10^{11}	Pa
Young's Modulus Z(T) direction	3×10^{8}		Pa
Poisson's Ratio XY	0.21		-
Poisson's Ratio YZ	0.21	0.3	-
Poisson's Ratio XZ	0.24		-
Shear Modulus XY	6.5×10^{8}		Pa
Shear Modulus YZ	6.5×10^{8}	7.692×10^{11}	Pa
Shear Modulus XZ	6.5×10^{8}		Pa
Tensile Yield Strength	2.4×10^{7}	2.5×10^{8}	Pa
Compressive Yield Strength	3×10^{8}	2.5×10^{8}	Pa

3.3. Mesh element type

For the meshing of each model, quadrilateral element types are used instead of triangular because of their ability to capture the geometry response accurately and to give a good representation of the actual deformation. Details regarding the type of the element used are provided in Table 5.

Table 5. Element type details

Part	Element name IDs	Element shape
Plates	SHELL181	QUAD4
Beams	BEAM188	BEAM3

3.4. Design criteria

To ensure the robustness of the hybrid design, the following criteria must be fulfilled:

- Glulam under combined bending and axial tension criteria [12]

Criteria 1
$$\frac{\sigma_{t,0,d}}{f_{t,0,d}} + \frac{\sigma_{m,y,d}}{f_{m,y,d}} + k_m.\frac{\sigma_{m,z,d}}{f_{m,z,d}} \leq 1 \quad (1)$$

Criteria 2
$$\frac{\sigma_{t,0,d}}{f_{t,0,d}} + k_m.\frac{\sigma_{m,y,d}}{f_{m,y,d}} + \frac{\sigma_{m,z,d}}{f_{m,z,d}} \leq 1 \quad (2)$$

$\sigma_{t,0,d}$ is the design tensile stress along the grain, $\sigma_{m,y,d}$ and $\sigma_{m,z,d}$ are the design bending stresses around the y and z axes, $f_{t,0,d}$ is the design tensile stress along the grain, $f_{m,y,d}$, and $f_{m,z,d}$ are the corresponding design bending strengths, and k_m is a factor that makes allowance for the re-distribution of stresses and the effect of inhomogeneities of the material, and is 0.7 for glulam with a rectangular cross-section.

- Glulam under combined bending and axial compression criteria [12]

Criteria 3
$$\left(\frac{\sigma_{c,0,d}}{f_{c,0,d}}\right)^2 + \frac{\sigma_{m,y,d}}{f_{m,y,d}} + k_m.\frac{\sigma_{m,z,d}}{f_{m,z,d}} \leq 1 \quad (3)$$

Criteria 4
$$\left(\frac{\sigma_{c,0,d}}{f_{c,0,d}}\right)^2 + k_m.\frac{\sigma_{m,y,d}}{f_{m,y,d}} + \frac{\sigma_{m,z,d}}{f_{m,z,d}} \leq 1 \quad (4)$$

Where $\sigma_{c,0,d}$ is the design compressive stress along the grain, $f_{c,0,d}$ is the design's compressive strength along the grain.

- Glulam beam stability criteria [12]

Criteria 5
$$\left(\frac{\sigma_{m,d}}{k_{crit}.f_{m,d}}\right)^2 + \frac{\sigma_{c,0,d}}{k_{c,z}.f_{c,0,d}} \leq 1 \quad (5)$$

Where $\sigma_{m,d}$ is the design bending stress, k_{crit} is a factor that considers the reduced bending strength due to lateral buckling, and $k_{c,z}$ is an instability factor. The values of k_{crit} and $k_{c,z}$ can be calculated based on equations given in EN 1995-1-1 standard [12].

- Steel plates yielding criteria [13]

Criteria 6
$$\gamma_m \frac{\sigma_{j,d}}{R_k} \leq 1 \quad (6)$$

$\sigma_{j,d}$ is von Mises equivalent design stress, R_k is the characteristic strength, and $\gamma_m = 1.15$ taken for plated structures.

In order to simplify the analysis of the design, only 6 output variables corresponding to the left side of each of the six design criteria are evaluated. The left side of each of the criteria represents the beam's utilization factor (UF).

Figure 4 shows the utilization factor according to the 1st criteria for configuration (b), while Table 6 presents a comparison between the maximum utilization factor for each configuration based on the above-mentioned criteria. The results show that configuration (b) provides an accepted utilization factor with minimal glulam mass. Therefore, all further results will be presented for configurations (b) only.

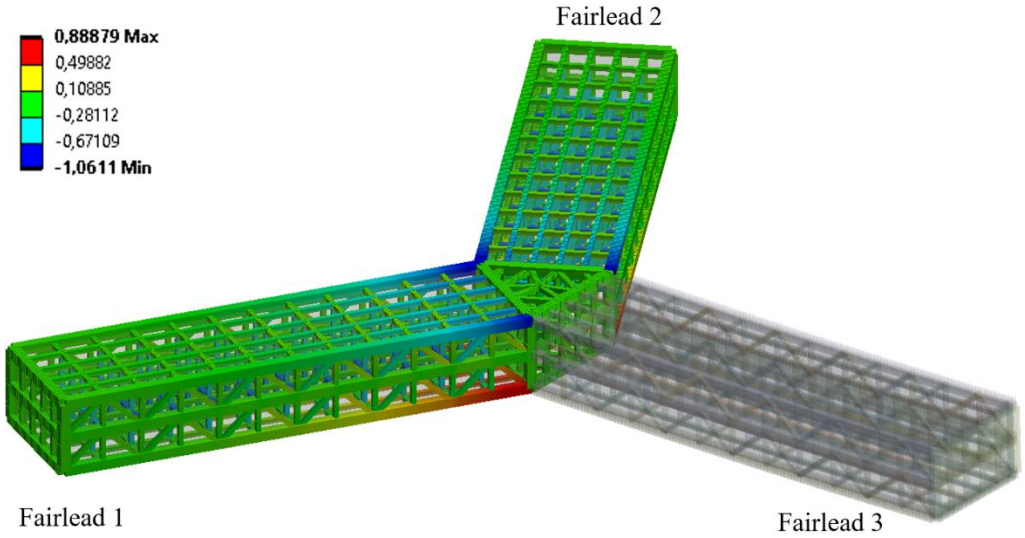

Figure 4. Utilization factor corresponding to the 1st combined bending and tension criteria for glulam, configuration (b)

Table 6. Max utilization factor for three hybrid configurations

Material	Design criteria	Config. (a)	Config. (b)	Config. (c)
Glulam	$UF_{max,\ 1}$	1.03	0.75	0.76
	$UF_{max,\ 2}$	1.04	0.80	0.82
	$UF_{max,\ 3}$	5.63	0.90	0.94
	$UF_{max,\ 4}$	5.36	0.90	0.94
	$UF_{max,\ 5}$	1.13	0.89	0.88
Steel	$UF_{max,\ 6}$	3.60	0.91	0.83

4. Hydro-Servo-Aero-Elastic analysis using OpenFAST

OpenFAST, an open-source simulation tool developed by the National Renewable Energy Laboratory (NREL), is utilized in this work for the fully coupled aero-hydro-elastic-servo dynamic analysis of the 15-MW FWT. The OpenFAST code couples together several computer codes such as AeroDyn [14], HydroDyn [15], ServoDyn, ElastoDyn, TurbSim, InflowWind, and MoorDyn [16], to account for the aerodynamic loads on rotor blades, hydrodynamic loads on floaters, control dynamics, structural dynamics, and mooring system dynamics.

According to Yousef [10], the hybrid floater has CoB, CoG, mass, and moments of inertia identical to the UMaine VolturnUS-S platform with a significant decrease in the mass of steel and concrete. Additionally, the hybrid floater's external dimensions and geometry are identical to those of the UMaine VolturnUS-S platform. Based on that, the requirements for stability and eigenfrequency are automatically satisfied, and the hydrodynamic properties, that are already provided for the UMaine VolturnUS-S platform [9], can be directly used for the analysis of the hybrid floater configuration (b).

4.1. Design load cases (DLC)

The performance of the hybrid floater is evaluated using a subset of IEC design load cases that presents the U.S. East Coast [17, 18]. All simulations were carried out for 720 sec assuming that both wind and wave are aligned at 0 degree, see Table 7.

Table 7. IEC Design load cases

	DLC number	**Wind condition**	U_{hub} **(m/s)**	H_s **(m)**	T_p **(sec)**	**Gamma shape factor**
1.1	1	**NTM**	4.00	1.10	8.52	1.00
	2		24.00	4.52	9.45	1.89
1.3	3	**ETM**	4.00	1.10	8.52	1.00
	4		24.00	4.52	9.45	1.89
1.6	5	**NTM**	4.00	6.30	11.50	2.75
	6		24.00	9.80	14.10	2.75

where ETM is the Extreme turbulence model and NTM is the Normal turbulence model.

Using OpenFAST, all the total time-varying loads on the tower base and mooring line tension such as TwrBsFxt, TwrBsFyt, TwrBsFzt, TwrBsMxt, TwrBsMyt, TwrBsMzt, FAIRTEN1, FAIRTEN2 are obtained.

5. Local Analysis

5.1. FEA Model

Using the results obtained from OpenFAST, model (b) is re-analyzed using the actual loads, see Figure 5.

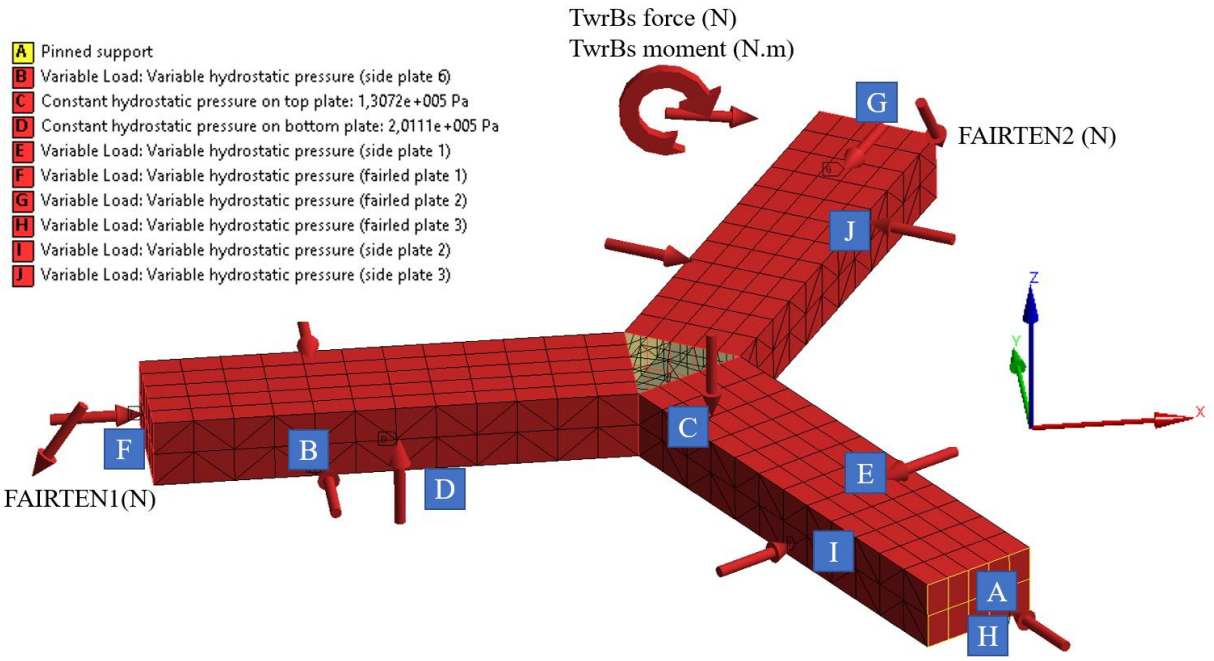

Figure 5. Actual loads acting on the hybrid design, configuration (b) (ANSYS)

5.2. Response Surface Methodology (RSM)

Response surface methodology (RSM) is a statistical method that can investigate the relationships between several inputs and one or more outputs based on mathematical regression. Response surface reduces the computational time by avoiding the need for running thousands of simulations based on the different load combinations (obtained at each time step Δt during the simulation length).

5.2.1. Design of experiment (DoE)

In ANSYS Workbench, there are many approaches to generate experimental design points, such as the Box-Behnken design, central composite design, optimal space-filling design, etc. Only the central composite design is taken into consideration for this paper. A set of 285 design points is generated based on the upper and lower bound presented in Table 8.

Table 8. Upper and lower bounds assigned for input load variables

	TwrBsFxt	**TwrBsFyt**	**TwrBsFzt**	**TwrBsMxt**
Lower bound	-3×10^6	-2×10^6	-3×10^7	-8×10^7
Upper bound	9×10^6	2×10^6	3×10^7	2×10^8
	TwrBsMyt	**TwrBsMzt**	**FAIRTEN1**	**FAIRTEN2**
Lower bound	-4×10^8	-4×10^7	1×10^6	1×10^6
Upper bound	7×10^8	4×10^7	6×10^6	3×10^6

5.2.2. Construction of response surface

In ANSYS Workbench, the response surface can be built in a variety of ways, including Kriging, conventional second-order regression, non-parametric regression, etc. This paper uses generic aggregation to generate the response surface, which uses a genetic algorithm to simultaneously solve many response surfaces while considering the stability and correctness of the response surface at the design point. Eq. (7) provides the mathematical description of the generic aggregation approach.

$$\hat{y}_{ens}(x) = \sum_{i=1}^{N_m} w_i \cdot \hat{y}_i(x) \quad (7)$$

Where $\hat{y}_{ens}$ is the ensemble prediction, N_m is the total number of metamodels used and $\hat{y}_i$, w_i are the prediction and weight factor of the $i-th$ response surface.

The results obtained from goodness of fit option available in ANSYS workbench show that the generated response surface provides a good fit to the model studied, see Table 9.

Table 9. Goodness of fit results

	$UF_{max,\ 1}$	$UF_{max,\ 2}$	$UF_{max,\ 3}$	$UF_{max,\ 4}$	$UF_{max,\ 5}$	$UF_{max,\ 6}$
Coefficient of Determination (best value=1)						
Learning Points	1	0.999	0.999	1	0.999	1
Cross-Validation on Learning Points	0.979	0.990	0.946	0.907	0.957	0.948
Maximum Relative Residual (best value=0%)						
Learning Points	0	0.208	0.055	0	0.183	0
Verification Points	3.221	1.755	7.290	6.449	3.183	1.564
Cross-Validation on Learning Points	2.726	2.185	7.172	8.251	4.040	1.818
Root Mean Square Error (best value=0)						
Learning Points	0	0	0	0	0	0
Verification Points	0.017	0.009	0.027	0.032	0.014	0.006
Cross-Validation on Learning Points	0.003	0.003	0.009	0.01	0.005	0.002
Relative Root Mean Square Error (best value=0%)						
Learning Points	0	0.048	0.04	0	0.059	0
Verification Points	2.164	1.188	3.907	4.253	1.667	0.797
Cross-Validation on Learning Points	0.397	0.41	1.122	1.201	0.517	0.239

5.3. Parameter correlation study

The aim of the correlation study is to reduce the total computational time by detecting which of the inputs have the greatest influence on the output. This makes it possible to identify the worst-case load combinations while considering fewer inputs at their maximum/minimum values.

Results from the correlation study showed that the correlation coefficients between the load input variables and the output stress variables vary significantly based on the direction of each individual load [10]. However, the study highlighted that some inputs such as TwrBsFxt, TwrBsFzt, TwrBsMyt, FAIRTEN1, FAIRTEN1, and FAIRTEN2 have significant influence in the output, and must be considered during the process of selecting the worst-case load combinations, see [10].

5.4. Results

The maximum utilization factors for each of the design load cases are shown in Table 10 based on the worst-case load combinations. Each worst-case load combination corresponds to the maximum/minimum value for one of the input load variables. Then, the 6 utilization factors for each of

the selected load combinations are extracted using the response surface. The results show that the utilization of glulam beams reaches up to 85% as a result of the combined bending and tension, and up to 78% as a result of combined bending and compression. However, the beams reach 94% of their capacity while resisting buckling.

Table 10. The maximum utilization factors expected for each of the design loads

DLC number	Wind condition	Glued laminated timber					Steel
		$UF_{max,\ 1}$	$UF_{max,\ 2}$	$UF_{max,\ 3}$	$UF_{max,\ 4}$	$UF_{max,\ 5}$	$UF_{max,\ 6}$
1	NTM	0.7679	0.8175	0.7417	0.7548	0.9085	0.8153
2		0.7908	0.8406	0.7793	0.7763	0.9339	0.8243
3	ETM	0.7776	0.8280	0.7581	0.7633	0.9196	0.8194
4		0.7914	0.8414	0.7805	0.7767	0.9349	0.8246
5	NTM	0.7834	0.8331	0.7667	0.7690	0.9253	0.8213
6		0.7943	0.8436	0.7834	0.7804	0.9372	0.8256

6. Conclusion

This paper presents a new hybrid timber-steel floating substructure for a 15 MW semi-submersible-type FWT. Based on a set of assumptions, A preliminary design study was conducted by modelling and comparing the 3 FE model using ANSYS Workbench 2020 R1. The results show that configuration (b) offers acceptable utilization factors with minimal glulam mass (cost). Furthermore, the selected hybrid design saves about 590 t of steel mass in comparison to the UMaine VolturnUS-S semi-submersible platform. Based on the similarity in geometry, mass properties, CoG, and CoB, the hydrodynamic properties provided for the UMaine VolturnUS-S semi-submersible platform [9] were utilized to perform a fully nonlinear aero-hydro-servo-elastic simulation of the hybrid model (b). Subsequently, Model (b) was re-analyzed using the actual loads produced by OpenFAST. Response surface methodology is then used to minimize the overall calculation time. To detect worst-case load combinations (inputs) that provide maximum utilization factors (outputs), a parameter correlation study was conducted. The parameter correlation study's findings revealed a substantial varying correlation between TwrBsFxt, TwrBsFzt, TwrBsMyt, FAIRTEN1, FAIRTEN1, FAIRTEN2, and the resulting utilization factors. The final results show that glulam can offer a good alternative for structural steel for IEA 15 MW with a utilization factor that varies between 0.74-0.94 for the different criteria under normal and extreme operating conditions. The insignificant difference in the utilization factor values among the different DLC emphasizes the importance of hydrostatic pressure as a design-driving load.

Reference

[1] IEA, “World energy outlook 2020. OECD Publishing,” 2020.

[2] WindEurope, *Floating offshore wind energy-a policy blueprint for europe floating offshore wind energy* 2018.

[3] J. Igba, K. Alemzadeh, C. Durugbo, and K. Henningsen, “Performance assessment of wind turbine gearboxes using in-service data: Current approaches and future trends,” *Renewable and Sustainable Energy Reviews,* vol. 50, pp. 144-159, 2015-10-01, 2015.

[4] R. Pulselli, M. Maccanti, M. Bruno, A. Sabbetta, E. Neri, N. Patrizi, and S. Bastianoni, “Benchmarking Marine Energy Technologies Through LCA: Offshore Floating Wind Farms in the Mediterranean. Front,” *Perspectives for marine energy in the mediterranean area volume II,* vol. 16648714, pp. 18, 2023.

[5] J. Porteous, and A. Kermani, *Structural timber design to Eurocode 5*: John Wiley & Sons, 2013.

[6] R. Abrahamsen, "Mjøstårnet-Construction of an 81 m tall timber building."
[7] Modvion, "The first wooden wind power tower has been erected in Sweden," 29 April 2020.
[8] E. Gaertner, J. Rinker, L. Sethuraman, F. Zahle, B. Anderson, G. E. Barter, N. J. Abbas, F. Meng, P. Bortolotti, and W. Skrzypinski, *IEA wind TCP task 37: definition of the IEA 15-megawatt offshore reference wind turbine*, National Renewable Energy Lab.(NREL), Golden, CO (United States), 2020.
[9] C. Allen, A. Viscelli, H. Dagher, A. Goupee, E. Gaertner, N. Abbas, M. Hall, and G. Barter, *Definition of the UMaine VolturnUS-S reference platform developed for the IEA Wind 15-megawatt offshore reference wind turbine*, National Renewable Energy Lab.(NREL), Golden, CO (United States); 2020.
[10] H. H. Yousef, "Design and analysis of a hybrid timber-steel floating substructure for a 15 MW semi-submersible-type FWT," (Master Thesis), University of Stavanger 2023.
[11] European Committee for Standardization CEN, "NS-EN 14080: 2013 NA: 2016 Timber structures-Glued laminated timber and glued solid timber Requirements," 2013.
[12] European Committee for Standardization CEN, "Eurocode 5: Design of timber structures - Part 1-1: General -Common rules and rules for buildings," EN, 2006.
[13] Det Norske Veritas (DNV), "DNV-OS-C101: Design of Offshore Steel Structures General (LRFD Method)," 2011.
[14] P. J. Moriarty, and A. C. Hansen, *AeroDyn Theory Manual,* NREL/TP-500-36881, National Renewable Energy Lab., Golden, CO (US), 2005.
[15] National Renewable Energy Laboratory (NREL). "OpenFAST Documentation," 12.04.2023; https://openfast.readthedocs.io/en/dev/index.html.
[16] M. Hall, "MoorDyn user's guide," *Department of Mechanical Engineering, University of Maine: Orono, ME, USA,* vol. 15, 2015.
[17] A. M. Viselli, A. J. Goupee, and H. J. Dagher, "Model test of a 1: 8-scale floating wind turbine offshore in the gulf of maine," *Journal of Offshore Mechanics and Arctic Engineering,* vol. 137, no. 4, 2015.
[18] G. M. Stewart, A. Robertson, J. Jonkman, and M. A. Lackner, "The creation of a comprehensive metocean data set for offshore wind turbine simulations," *Wind Energy,* vol. 19, no. 6, pp. 1151-1159, 2016.